

1 **Australian plate subduction is responsible for northward motion of the India-Asia collision zone**
2 **and ~1000 km lateral migration of the Indian slab**

3
4 **Parsons AJ¹, Sigloch K^{1,2}, Hosseini K^{1,3}.**

5 *Author affiliations:*

- 6 1. *Dept. Earth Sciences, University of Oxford, Oxford, UK.*
7 2. *Université Côte d'Azur, CNRS UMR 7329, Géoazur, Sophia Antipolis, France*
8 3. *Alan Turing Institute, London, UK*

9
10 **Key Points**

- 11 • **Subduction of Australian oceanic lithosphere drove northward motion of coupled India-**
12 **Australia plate since onset of collision at 45-40 Ma**
13 • **Buoyant Indian continent stalled subduction of Indian slab whilst Australian slab**
14 **subduction drove motion of coupled India-Australia plate**
15 • **~1000 km north lateral migration of Indian slab occurred to maintain compatibility with**
16 **plate kinematics of coupled India-Australia plate**

17
18
19 **Plain Language Summary**

20 To understand the links between plate tectonics and mantle processes, researchers must determine
21 how tectonic plates have moved with respect to the evolving mantle through geological time. To
22 overcome this problem, recent studies use the locations of subducted slabs in the deep mantle to
23 reconstruct plate motions, based on the hypothesis that slabs sink vertically through the mantle, and
24 therefore mark the surface locations of past subduction zones. Here, we test slab sinking
25 hypotheses, and their use in plate reconstruction modelling, by investigating the sinking kinematics
26 of the subducting Indian and Australian slabs during the India-Asia collision. Our analysis indicates
27 that since onset of collision at ~45-40 Ma, the Indian slab migrated laterally, ~1000 km northwards
28 through the mantle, driven by subduction of the neighbouring Australian slab. We arrive at this new
29 interpretation because we interpret Indian and Australian slab kinematics collectively, and with
30 respect to India-Australia plate motions. Our study shows that the sinking behaviour of one slab can
31 influence that of another slab in the same network. Slab-based plate reconstructions should
32 therefore interpret slabs of the same network collectively, and with respect to plate motions, in
33 order to constrain non-vertical slab motions and avoid potentially significant plate reconstruction
34 errors.

35

36 **Abstract**

37 Distributions of slabs within Earth's mantle are increasingly used to reconstruct past subduction
38 zones, based on first-order assumptions that slabs sink vertically after slab break-off, and thus
39 delineate paleo-trench locations. Non-vertical slab motions, which occur prior to break-off,
40 represent a potentially significant source of error for slab-based plate reconstructions, but are
41 poorly understood. We constrain lateral migration of the Indian slab and overlying India-Asia
42 collision zone by comparing tomographically-imaged mantle structure with plate-kinematic
43 constraints. Following coupling of the Indian and Australian plates at the onset of collision, ~1000 km
44 lateral migration of the Indian slab was driven by vertical subduction of the Australian slab. The
45 sinking behaviours of individual slabs do not evolve in isolation, but instead influence, or are
46 influenced by, other slabs in the same plate network. Hence, lateral slab migrations may be
47 determined by interpreting the sinking behaviour of slabs collectively, and with respect to plate
48 kinematics.

49

50

51

52

53 The ultimate goal of tectonic plate reconstruction modelling is to constrain absolute motions of
54 Earth's continents and oceans, with respect to the mantle, through geological time (Torsvik et al.,
55 2008, van der Meer et al., 2010, Doubrovine et al., 2012). This is crucial to our understanding of how
56 surface processes, plate tectonics, and mantle dynamics link at a planetary scale (Steinberger et al.,
57 2012, Domeier et al., 2016), and essential for the ability to test working hypotheses against bedrock
58 and mantle records (Wu et al., 2016, Sigloch and Mihalynuk, 2017, van de Lagemaat et al., 2018,
59 Clennett et al., 2020, Fuston and Wu, 2020, Parsons et al., 2020). Absolute plate motions are
60 constrained using a mantle reference frame, based primarily on the tracking of oceanic plates across
61 mantle hot-spots (Torsvik et al., 2008, Doubrovine et al., 2012). However, hot-spot tracks do not
62 extend beyond ~130 Ma, which increases the uncertainty of absolute reconstructions of earlier
63 times (Doubrovine et al., 2012, Domeier et al., 2016). Development of a mantle reference frame that
64 uses subducted slabs as fixed reference points is a highly desirable solution to this problem, because
65 the widespread distribution and longer-term residency of slabs in the lower mantle should allow us
66 to reconstruct absolute plate motions with greater accuracy, back to at least 200-300 Ma (van der
67 Meer et al., 2010, Steinberger et al., 2012, Domeier et al., 2016, van der Meer et al., 2018).

68 Tomographically constrained, slab-based plate reconstructions are typically founded on an
69 assumption that after slab break-off, detached slabs sink vertically, such that the top of a detached
70 slab constrains the surface location of its subduction zone trench, at point of break-off
71 (Hafkenscheid et al., 2006, van der Meer et al., 2010, Steinberger et al., 2012, Replumaz et al., 2014,
72 Domeier et al., 2016, Wu et al., 2016, Parsons et al., 2020). Prior to slab break-off, the potential for
73 horizontal slab motions *during* subduction is poorly constrained, but has been shown to produce
74 significant errors in slab-based reconstructions if overlooked (Schellart, 2005, van de Lagemaat et al.,
75 2018).

76 Lateral slab migration (LSM) refers to a horizontal component of motion of part of, or all of, a slab,
77 which occurs during subduction, prior to slab break-off, and with respect to the surrounding mantle.
78 Numerical and analogue modelling suggest that LSM can occur in the upper mantle, where the
79 viscosity of a slab may force it to migrate perpendicular to the trench, towards or away from the
80 direction of subduction, as the slab bends and steepens (Schellart, 2005, Schellart et al., 2008,
81 Capitanio and Morra, 2012, Čížková and Bina, 2013, Holt et al., 2018). Such migrations are predicted
82 on the order of a few hundreds of kilometres and are typically accompanied by trench migration
83 (Schellart, 2005, Schellart et al., 2008, Holt et al., 2018). Within the lower mantle, modelling suggests
84 that slabs sink vertically (Steinberger et al., 2012, Čížková and Bina, 2013) with minor LSM on the
85 order of ~100-200 km per 100 Myrs (Steinberger et al., 2012).

86 LSMs inferred from observations of subducted slabs are uncommon (Le Dain et al., 1984, Giardini
87 and Woodhouse, 1986, Liu et al., 2008, Spakman et al., 2018, van de Lagemaat et al., 2018), and in
88 some cases disputed (Liu et al., 2008, Sigloch and Mihalynuk, 2017). Most notably, van de Lagemaat
89 et al. (2018) demonstrate ~1200 km of trench-parallel LSM of the Pacific slab beneath the Kermadec
90 arc since ~30 Ma, which was previously unaccounted for by plate reconstructions. Importantly,
91 magnitudes and directions of LSM inferred from natural examples have been shown to correspond
92 to absolute plate motion of the subducting plate (Spakman et al., 2018, van de Lagemaat et al.,
93 2018). This implies that within a single plate network, slab sinking (prior to break-off) and absolute
94 plate motions are related to each other. If this is correct, it should be possible to constrain
95 components of LSM from multiple slabs of the same network, by interpreting their sinking
96 kinematics collectively, and as connected parts that maintain compatibility with plate kinematics
97 during subduction. To test this hypothesis, we investigate the subduction kinematics of the India-
98 Asia collision (Fig. 1), where LSM has been proposed previously, but not constrained (Le Dain et al.,
99 1984, Parsons et al., 2020). We integrate seismic tomography (Fig. 2) with bedrock and plate-
100 kinematic constraints to constrain the kinematics of the Australian and Indian slabs during the India-
101 Asia collision (Fig. 3). By interpreting the size, distribution and morphology of these slabs collectively,
102 we propose that subduction of the Australian slab provided the driving force for ~1000 km
103 northward LSM of the Indian slab (Fig. 4).

104

105 **Plate network configurations for the India-Asia collision**

106 Several hypotheses have been proposed for the India-Asia collision, which vary in terms of timing
107 and number of collisions. Single-collision hypotheses propose a single, continuous collision between
108 India and Asia, which initiated at 59 ± 1 Ma (Hu et al., 2016, Ingalls et al., 2016). Double-collision
109 hypotheses argue for distinct collisional events at 59 ± 1 Ma (“First Collision”) and ~45-40 Ma
110 (“Second Collision”) (Patriat and Achache, 1984, Bouilhol et al., 2013, Jagoutz et al., 2015, van
111 Hinsbergen et al., 2019). Double-collision Hypothesis I proposes “First Collision” between India and
112 an equatorial intra-oceanic arc, followed by “Second Collision” between India-plus-arc and Eurasia
113 (Patriat and Achache, 1984, Bouilhol et al., 2013, Jagoutz et al., 2015). Double-collision Hypothesis II
114 proposes “First Collision” between an India-derived microcontinent and Eurasia, followed by
115 “Second Collision” between India and the modified Eurasian margin (van Hinsbergen et al., 2019).
116 Based on the review of Parsons et al. (2020), our study analyses slab kinematics during the India-Asia
117 collision in the context of double-collision hypotheses I and II (Fig. 3) (Patriat and Achache, 1984,

118 Bouilhol et al., 2013, Jagoutz et al., 2015, van Hinsbergen et al., 2019). Single-collision hypotheses
119 require extreme magnitudes of continental subduction, do not fit restorations of Gondwana, offer
120 no explanation for the plate network reorganization at 45-40 Ma (detailed below), and are not
121 considered further (Parsons et al., 2020).

122 Between ~120-40 Ma, the Indian plate was bounded by north-south striking transform boundaries to
123 its west and east (Fig. 3); its eastern boundary, defined by the Wharton ridge (Fig. 1), formed a
124 transform-dominated spreading ridge (Jacob et al., 2014, Gibbons et al., 2015). During that period,
125 the adjacent Australian plate remained at a relatively fixed position (Torsvik et al., 2008). Bedrock
126 records along the southern Eurasian margin reflect the contrasting kinematics of the Indian and
127 Australian plates (Fig. 1). West of the Wharton ridge, subduction-related magmatism between
128 southwest Tibet and Thailand occurred throughout the Late Cretaceous to ~50-40 Ma (Morley, 2012,
129 Zhu et al., 2018, Lin et al., 2019). East of the Wharton ridge, northward subduction beneath Java and
130 Sulawesi ceased at ~90-80 Ma (Hall, 2012, Morley, 2012, Breithfeld et al., 2020), and re-initiated
131 beneath Java at 47-44 Ma (Smyth et al., 2008), coincident with onset of northward migration of the
132 Australian plate (Torsvik et al., 2008, Müller et al., 2019).

133 During the mid-Eocene, a significant plate network reorganization was recorded across the Indian
134 Ocean (Patriat and Achache, 1984, Gibbons et al., 2015) (Fig. 3c). This included: (1) 30-38% reduction
135 in Indian plate velocity between 45-40 Ma (Molnar and Stock, 2009); (2) cessation of Wharton ridge
136 spreading and subsequent coupling between Indian and Australian plates at ~43-36 Ma (Jacob et al.,
137 2014, Gibbons et al., 2015); (3) onset of Australian plate subduction beneath Java at 47-44 Ma
138 (Smyth et al., 2008); (4) onset of northward migration of the Australian plate at ~45-43 Ma (Torsvik
139 et al., 2008, Müller et al., 2019); (5) accelerated spreading between the Australian and Antarctic
140 plates at ~47-45 Ma (Torsvik et al., 2008, Eagles, 2019, Seton et al., 2020); (6) change in rates and
141 azimuths of spreading between India and Africa between 47-41 Ma (Patriat and Achache, 1984,
142 Cande et al., 2010, Seton et al., 2020); (7) southwestward jump of the Central India spreading ridge
143 at ~41 Ma (Torsvik et al., 2013). These well-constrained changes in plate kinematics and subduction
144 make the Indian and Australian plates and associated slabs a good target for testing whether LSMs
145 can be inferred by interpreting the kinematics of multiple slabs collectively, and with respect to plate
146 motions.

147

148 **Slab kinematics during the India-Asia collision**

149 We focus on two slabs of subducted lithosphere beneath southeast Asia (Anomaly VII) and northern
150 India (Anomaly II; *anomaly numbers follow Parsons et al., 2020*) (Fig. 2), based on combined
151 observations from six tomography models (Supporting Information and Dataset) (Amaru, 2007, Li et
152 al., 2008a, Simmons et al., 2012, Obayashi et al., 2013, Schaeffer and Lebedev, 2013, Hosseini et al.,
153 2020). Our interpretations of these slabs are supported by the most up-to-date, integrated
154 assessment of bedrock, subsurface and kinematic constraints from Tibet-Himalaya and central
155 Indian Ocean (Parsons et al., 2020). Further constraints are provided by our own integration of
156 bedrock and mantle records between Myanmar and Indonesia, and Australian plate kinematics (see
157 Supporting Information), which were not considered by previous tomographically-constrained
158 interpretations of the study region (Hafkenscheid et al., 2006; Replumaz et al., 2014; Parsons et al.,
159 2020).

160 Anomaly VII comprises Indian and Australian lithosphere presently subducting between Myanmar
161 and Indonesia and includes the extinct Wharton ridge (Figs. 1-2). Between Sumatra and Indonesia,
162 Anomaly VII forms a near-vertical slab from the trench down to ~800-1000 km depth, where it
163 thickens as it piles up in the mantle transition zone (MTZ) and lower mantle (Figs. 2i, S2j-q). Beneath
164 Myanmar and Thailand, Anomaly VII dips southwards (Fig. 2h). Parts of this western section of
165 Anomaly VII are doubly thickened with respect to its eastern section (Fig. S2i).

166 Anomaly II is a detached slab imaged in the MTZ and lower mantle beneath Tibet and northern India
167 (Fig. 2). Between ~450–550 km and ~800-1000 km depth, Anomaly IIa forms a NW-SE striking,
168 southwest dipping, linear anomaly (Fig. 2a). Between ~800-1000 km and ~1100-1300 km depth,
169 Anomaly IIb forms a wider, subhorizontal anomaly (Figs. 2b-d, 2g-h, S2e-g).

170 We integrate our analysis of Anomalies VII and II within a kinematic reconstruction of the Indian,
171 Australian and Eurasian plates at 59 Ma and 43 Ma (Fig. 3), corresponding to “First” and “Second”
172 collision, respectively (Patriat and Achache, 1984, Bouilhol et al., 2013). Our 59 Ma restoration (Fig.
173 3b) includes alternative plate-boundary configurations for both double-collision hypotheses (Patriat
174 and Achache, 1984, Bouilhol et al., 2013, Jagoutz et al., 2015, van Hinsbergen et al., 2019). Indian
175 and Australian plate motions are constrained by seafloor isochrons in a moving-hotspot reference
176 frame (Müller et al., 2019). The location and kinematics of the southern Eurasian subduction zone
177 are constrained from our tomography analysis (Figs. 2, S2-4), integrated with bedrock and plate-
178 kinematic constraints (Supporting Information).

179 First, we focus on the kinematics of the Anomaly VII slab (beneath Myanmar to Indonesia). The well-
180 defined morphology of Anomaly VII and its connectivity with the Indian and Australian plates (Figs 2i,
181 S2h-q) make it suitable for restoration to its pre-subduction horizontal length following methods
182 outlined by Hafkenscheid et al. (2006) and Wu et al. (2016) (methods detailed in supporting
183 information).

184 Figure 3a shows our maximum and minimum restored lengths of the Anomaly VII slab determined
185 from cross sections H to Q. Between cross sections J to Q, the length of lithosphere restored from
186 Anomaly VII (distance between yellow dots and grey-white dashed lines) is equivalent to the total
187 plate motion of the Australian plate, since ~43 Ma (Torsvik et al., 2008, Müller et al., 2019) (distance
188 between yellow and red dots). This equivalency between Anomaly VII slab volume and Australian
189 plate motion since ~43 Ma implies that Anomaly VII is not voluminous enough to account for
190 subduction beneath the southeast Eurasian margin *prior* to ~43 Ma. This geometry-based inference
191 is independent of, but consistent with (1) Late Cretaceous-Middle Eocene hiatus of subduction
192 beneath southeast Eurasia (Hall, 2012, Morley, 2012) during a period of relative immobility of the
193 Australian plate (Torsvik et al., 2008, Müller et al., 2019); followed by (2) onset of subduction
194 beneath Java (Smyth et al., 2008) and northward migration of the Australian plate (Torsvik et al.,
195 2008, Müller et al., 2019) at 47-43 Ma (Fig. 3c). Integrating these events with our restoration of
196 Anomaly VII suggests that the Eurasian margin between sections J to Q has been stationary since
197 ~90-80 Ma (Fig. 3a). This is consistent with the vertical morphology of Anomaly VII between sections
198 J to Q (Fig. 2i), which is most simply explained by subduction beneath a stationary trench with
199 negligible LSM. We therefore carry over our 43 Ma restoration of the Eurasian margin between
200 sections J to Q into our 59 Ma restoration (Fig. 3b).

201 On cross sections H and I, we interpret the southwards dip (Fig. 2h) and thickened geometry (Fig.
202 S2i) of Anomaly VII as a record of slab overturning (e.g. Schellart, 2005, Capitanio et al., 2015),
203 caused by northwards trench migration, during subduction. Assuming that the slab sank vertically as
204 it overturned, the southern basal edge of the slab marks the approximate location of the overlying
205 trench at the onset of subduction. From this, we estimate that since ~43 Ma, the Sunda-Andaman
206 trench has migrated ~800 km and ~300 km northeast along sections H (Fig. 2h) and I (Fig. S2i),
207 respectively. Incorporating our estimates of trench migration into our restoration demonstrates an
208 equivalency between Indian plate motion since ~43 Ma (distance between yellow and red dots) and
209 the combined length of [restored Anomaly VII slab] + [trench migration] from sections H and I
210 (distance between yellow dots and light blue-white dashed lines). Thus, at 43 Ma, we restore the
211 Sunda-Andaman trench overlying sections H and I, 800 km and 300 km southeast of its present day
212 location (orange dots, Fig 3a), along strike from the restored Eurasian margin between sections J to
213 Q.

214 Crucially, the restored 43 Ma Eurasian margin between sections H and I (orange dots, Fig. 3a)
215 coincides *spatially* with the reconstructed northern edge of Greater India (Fig. 3a) (constrained by
216 Parsons et al., 2020), and *temporally* with the 30-38% reduction in Indian plate velocity between
217 ~45-40 Ma (Molnar and Stock, 2009) (Fig. 3c). Hence, our restoration supports previous arguments
218 (Patriat and Achache, 1984, Bouilhol et al., 2013, Gibbons et al., 2015, Jagoutz et al., 2015) that
219 collision between India and Eurasia occurred at ~45-40 Ma (Fig. 3c). We therefore propose that at 43
220 Ma, the northern edge of Greater India was in contact with the Eurasian margin, and so we extend
221 our Eurasian margin restoration (red barbed line, Fig. 3a) westward from section H, coincident with
222 the edge of Greater India. Our restoration implies that since collision at ~43 Ma, the India-Eurasia
223 plate boundary west of section H has migrated ~1000-2000 km northeast to its present-day location,
224 defined by the Indus suture zone (ISZ, Fig. 3a). This is consistent with paleomagnetic constraints
225 which place southern Tibet at $20^{\circ}\text{N} \pm 4^{\circ}$ at ~52 Ma (Huang et al., 2015). A shapefile of our Eurasian
226 margin restoration is included in supplementary files.

227 We attribute differences in trench kinematics and slab morphology between sections H to I, and J to
228 Q, to the Wharton ridge, which we restore coincident with section J at 43 Ma and 59 Ma (Fig. 3a-b).
229 The Eurasian margin at sections H and I formed part of the longer lived subduction zone between
230 Myanmar-Thailand and southern Tibet that was responsible for subduction of the Indian \pm
231 Neotethys plate(s) from ~110 Ma to ~40 Ma (Zhu et al., 2018, Lin et al., 2019) (Fig. 3b). The
232 corresponding slab(s) associated with that subduction began subducting ~70 Myr earlier than the
233 Anomaly VII slab (Fig 3b), and hence should now be located deeper than Anomaly VII. We therefore
234 assign the Indian plate slab to Anomaly II (Fig. 3b), imaged beneath north India from ~450-550 km to
235 ~1000-1300 km depth (Fig. 2a-c,g-h). We are confident in this interpretation because it is the
236 simplest explanation for the whereabouts of the Indian plate slab, and because there are no other
237 oceanic basins that Anomaly II can be related to (Parsons et al., 2020).

238 Importantly, Anomaly II is presently located ~1000 km north of our 43 Ma restoration of the
239 Eurasian margin (Figs. 2g, 3a). Applying an assumption of vertical sinking with no LSM to Anomaly II
240 would contradict our restorations of the Eurasian and Indian margins, and from a kinematic
241 perspective, would delay contact between India and Eurasia by ~10-20 Myrs. We therefore propose
242 that since "Second Collision" at ~45-40 Ma, the Anomaly II slab has laterally migrated ~1000 km

243 northwards through the surrounding mantle (Figs 2g, 4). The south dipping morphology of Anomaly
244 II is consistent with slab-overturning during LSM (Figs. 2g, S2e-g).

245 Previous studies that did not consider the sinking kinematics of Anomaly VII in their investigations of
246 Anomaly II, did not detect LSM (Hafkenscheid et al., 2006, Replumaz et al., 2014). Instead, those
247 studies either located the ~60-45 Ma collision zone above present-day Anomaly II (Hafkenscheid et
248 al., 2006), which is inconsistent with the location of the northern Indian margin at that time (Fig. 3a-
249 b), or interpreted Anomaly II as subducted Indian and Asian *continental* lithosphere (Replumaz et al.,
250 2014), which is not robustly demonstrated by bedrock and geophysical observations (Parsons et al.
251 2020). Interpreting the Indian slab (Anomaly II) with respect to the Australian slab (Anomaly VII) and
252 the surrounding plate network, as we do, leads us to our new interpretation, which is supported by a
253 greater set of constraints.

254 Lastly, we note that our Eurasian margin restoration (red barbed line, Fig. 3a-b) is coincident with
255 Anomaly III (grey-dashed line, Fig. 3a), which forms a vertical slab-wall from ~800-950 km to ~1700-
256 1800 km depth (Fig. 2). We therefore propose that the southern Eurasian plate boundary formed a
257 subduction zone above Anomaly III, tens of millions of years prior to 59 Ma (Fig. 3b).

258 **Plate tectonic explanation for LSMs**

259 Our analysis suggests that east of the Wharton ridge, the Eurasian margin and Anomaly VII slab
260 remained at a relatively fixed location since ~43 Ma. At the same time, west of the Wharton ridge,
261 the Anomaly II slab laterally displaced by ~1000 km, and the Anomaly VII slab overturned as the
262 overlying India-Asia collision zone migrated ~1000-2000 km northwards (Fig. 4).

263 Our interpretation is consistent with numerical models, which propose northward migration of the
264 India-Asia collision zone was driven by Australian plate subduction (e.g. Capitanio et al., 2015).
265 Consistent with those models, we propose that following Second Collision at ~45-40 Ma (Fig. 4a),
266 wholesale motion of the newly coupled India-Australia plate was driven by slab-pull of the
267 subducting Australian oceanic lithosphere (Anomaly VII-Aus, Fig. 4) (e.g. Li et al., 2008b, Capitanio et
268 al., 2015), whilst to the west, buoyancy of the Indian continent stalled Indian-plate subduction (Fig.
269 4a-c). To maintain compatibility between slab kinematics and plate kinematics, the Indian continent
270 was forced northwards, dragging the Indian oceanic slab with it (Anomaly II, Fig. 4b-c). Within the
271 mantle, the laterally migrating Indian slab (Anomaly II) separated from the vertically sinking
272 Australian oceanic slab (Anomaly VII-Aus, Fig.4b-c) along the subducted portion of the Wharton
273 ridge (Fig. 4b-c).

274 During northward migration of the Anomaly II slab and the India-Asia collision zone, Indian oceanic
275 lithosphere between India and the Wharton ridge overturned during subduction (Anomaly VII-Ind,
276 Figs. 2i, 4b-c), whilst the overlying subduction zone between Myanmar and Sumatra rotated
277 clockwise (around a vertical axis) and lengthened via NW-SE transform faulting (Fig. 4a-c). We
278 interpret the present-day location of Anomaly II as the location of complete Indian slab break-off
279 from the Indian continent, corresponding to a restoration age of ~30-25 Ma (Fig. 4b-c).

280 We build upon the observations of Replumaz et al. (2014), who recognised an overturned slab in the
281 upper mantle beneath India, by *kinematically* demonstrating that (1) Anomaly II is an oceanic slab,
282 which was dragged ~1000 km northwards during collision; and (2) timing and duration of Anomaly II

283 LSM coincided with the timing and duration of Australian plate subduction. Our study also
284 demonstrates that onset of subduction of the Australian plate coincided with plate network
285 reorganization in the Indian Ocean (Fig. 3c), including: (1) reorientation of Indian plate-motion
286 azimuth, from 000-020° to 020-040° (Torsvik et al., 2008, Gibbons et al., 2015, Müller et al., 2019);
287 and (2) changes in rates and azimuths of spreading between the Indian and African plates (Patriat
288 and Achache, 1984, Cande et al., 2010, Torsvik et al., 2013, Seton et al., 2020) and between the
289 Australian and Antarctic plates (Torsvik et al., 2008, Eagles, 2019, Seton et al., 2020) (Fig. 3c). Based
290 on an understanding that slab-pull is the dominant force behind plate motions (Forsyth and Uyeda,
291 1975), we postulate that these kinematic changes occurred in response to the onset of Australian
292 slab subduction.

293 **Conclusions**

294 We believe this is the first kinematically-constrained demonstration of significant LSM reported (1)
295 from a now-detached slab; and (2) in a trench-forward direction. Our findings demonstrate that
296 magnitudes of LSM prior to slab break-off can be large, and will produce errors in slab-based plate
297 reconstructions if overlooked. An assumption of vertical sinking applied to the Indian slab (Anomaly
298 II) would reconstruct the Eurasian margin directly above Anomaly II, which is incompatible with our
299 interpretation of the Australian slab (Anomaly VII), our restoration of the Eurasian and Indian
300 margins, and from a kinematic perspective, would delay collision by ~10-20 Myrs. Instead, we have
301 demonstrated that the Indian slab migrated ~1000 km laterally through the mantle since collision
302 between India and Eurasia at 45-40 Ma.

303 Previous studies, did not detect LSM because they did not consider the kinematics of Anomaly VII
304 (Australian slab) in their interpretations of Anomaly II (Indian slab). We arrive at our new
305 interpretation because, (1) we interpreted the distribution and geometry of subducted slabs as
306 integrated parts of a larger system (rather than in isolation); and (2) we expanded our region of
307 interest to include the Myanmar-to-Indonesia margin and Australian plate kinematics, to ensure that
308 our interpretations maintained compatibility between slab kinematics and plate kinematics.

309

310

311 **Acknowledgements**

312 For the purpose of review, data presented in this study are available in the supporting information.
313 Upon acceptance, data presented in this study will be hosted and made freely available at the
314 Oxford University Research Archive (ORA). We thank editor Lucy Flesch and reviewers Jon Pownall
315 and Fabio Capitanio for constructive reviews that improved our study. We thank Jonny Wu and
316 Richard Palin for helpful discussions regarding slab densities and slab area to plate area conversions.
317 We thank Graeme Eagles and Lucia Perez-Diaz for helpful discussions regarding the plate tectonic
318 evolution of the Indian Ocean. This work was supported by funding from the European Research
319 Council (ERC) under the European Union's Horizon 2020 research and innovation programme (grant
320 agreement 639003 "DEEP TIME").

321

322 Amaru, M. 2007. *Global travel time tomography with 3-D reference models*. Utrecht University.

323 Barber, A.J., Khin Zaw & Crow, M.J. 2017. Chapter 31: The pre-Cenozoic tectonic evolution of
324 Myanmar. In: Barber, A. J., Khin Zaw & Crow, M. J. (eds.) *Myanmar: Geology, Resources and*
325 *Tectonics*. Geological Society, London, Memoirs, 48, 687-712.

326 Barley, M.E., Pickard, A.L., Zaw, K., Rak, P. & Doyle, M.G. 2003. Jurassic to Miocene magmatism and
327 metamorphism in the Mogok metamorphic belt and the India-Eurasia collision in Myanmar.
328 *Tectonics*, 22.

329 Bergman, S.C., Coffield, D.Q., Talbot, J.P. & Garrard, R.A. 1996. Tertiary Tectonic and magmatic
330 evolution of western Sulawesi and the Makassar Strait, Indonesia: evidence for a Miocene
331 continent-continent collision. *Geological Society, London, Special Publications*, 106, 391-429.

332 Bertrand, G., Rangin, C., Maluski, H. & Bellon, H. 2001. Diachronous cooling along the Mogok
333 Metamorphic Belt (Shan scarp, Myanmar): the trace of the northward migration of the
334 Indian syntaxis. *Journal of Asian Earth Sciences*, 19, 649-659.

335 Bertrand, G. & Rangin, C. 2003. Tectonics of the western margin of the Shan plateau (central
336 Myanmar): implication for the India–Indochina oblique convergence since the Oligocene.
337 *Journal of Asian Earth Sciences*, 21, 1139-1157.

338 Bird, P. 2003. An updated digital model of plate boundaries. *Geochemistry, Geophysics, Geosystems*,
339 4.

340 Bouilhol, P., Jagoutz, O., Hanchar, J.M. & Dudas, F.O. 2013. Dating the India–Eurasia collision through
341 arc magmatic records. *Earth and Planetary Science Letters*, 366, 163-175.

342 Breitfeld, H.T., Davies, L., Hall, R., Armstrong, R., Forster, M., Lister, G., Thirlwall, M., Grassineau, N.,
343 Hennig-Breitfeld, J. & van Hattum, M.W.A. 2020. Mesozoic Paleo-Pacific Subduction Beneath
344 SW Borneo: U-Pb Geochronology of the Schwaner Granitoids and the Pinoh Metamorphic
345 Group. *Frontiers in Earth Science*, 8.

346 Brook, M. & Snelling, N. 1976. K/Ar and Rb/Sr age determinations on rocks and minerals from
347 Burma. *Report of the Isotope Geology Unit*, 76, 12.

348 Burg, J.-P. & Bouilhol, P. 2018. Timeline of the South-Tibet--Himalayan belt: the geochronological
349 record of subduction, collision, and underthrusting from zircon and monazite U-Pb ages.
350 *Canadian Journal of Earth Sciences*.

351 Cande, S.C., Patriat, P. & Dymant, J. 2010. Motion between the Indian, Antarctic and African plates in
352 the early Cenozoic. *Geophysical Journal International*, 183, 127-149.

353 Capitano, F.A. & Morra, G. 2012. The bending mechanics in a dynamic subduction system:
354 Constraints from numerical modelling and global compilation analysis. *Tectonophysics*, 522-
355 523, 224-234.

356 Capitano, F.A., Replumaz, A. & Riel, N. 2015. Reconciling subduction dynamics during Tethys closure
357 with large-scale Asian tectonics: Insights from numerical modeling. *Geochemistry,*
358 *Geophysics, Geosystems*, 16, 962-982.

359 Čížková, H. & Bina, C.R. 2013. Effects of mantle and subduction-interface rheologies on slab
360 stagnation and trench rollback. *Earth and Planetary Science Letters*, 379, 95-103.

361 Clennett, E.J., Sigloch, K., Mihalynuk, M.G., Seton, M., Henderson, M.A., Hosseini, K.,
362 Mohammadzaheri, A., Johnston, S.T. & Müller, R.D. 2020. A Quantitative Tomotectonic Plate
363 Reconstruction of Western North America and the Eastern Pacific Basin. *Geochemistry,*
364 *Geophysics, Geosystems*, 21, e2020GC009117.

365 Crow, M.J. & Khin Zaw 2017. Appendix: Geochronology in Myanmar (1964–2017). In: Barber, A. J.,
366 Zaw, K. & Crow, M. J. (eds.) *Myanmar: Geology, Resources and Tectonics*. Geological Society,
367 London, Memoirs. 48, 713-759.

368 Domeier, M., Doubrovine, P.V., Torsvik, T.H., Spakman, W. & Bull, A.L. 2016. Global correlation of
369 lower mantle structure and past subduction. *Geophysical Research Letters*, 43, 4945-4953.

370 Doubrovine, P.V., Steinberger, B. & Torsvik, T.H. 2012. Absolute plate motions in a reference frame
371 defined by moving hot spots in the Pacific, Atlantic, and Indian oceans. *Journal of*
372 *Geophysical Research: Solid Earth*, 117.

373 Dziewonski, A.M. & Anderson, D.L. 1981. Preliminary reference Earth model. *Physics of the Earth and*
374 *Planetary Interiors*, 25, 297-356.

375 Eagles, G. 2019. A little spin in the Indian Ocean plate circuit. *Tectonophysics*, 754, 80-100.

376 Forsyth, D. & Uyeda, S. 1975. On the Relative Importance of the Driving Forces of Plate Motion*.
377 *Geophysical Journal of the Royal Astronomical Society*, 43, 163-200.

378 Fuston, S. & Wu, J. 2020. Raising the Resurrection plate from an unfolded-slab plate tectonic
379 reconstruction of northwestern North America since early Cenozoic time. *GSA Bulletin*.

380 Gardiner, N.J., Roberts, N.M.W., Morley, C.K., Searle, M.P. & Whitehouse, M.J. 2016a. Did Oligocene
381 crustal thickening precede basin development in northern Thailand? A geochronological
382 reassessment of Doi Inthanon and Doi Suthep. *Lithos*, 240-243, 69-83.

383 Gardiner, N.J., Searle, M.P., Morley, C.K., Whitehouse, M.P., Spencer, C.J. & Robb, L.J. 2016b. The
384 closure of Palaeo-Tethys in Eastern Myanmar and Northern Thailand: New insights from
385 zircon U–Pb and Hf isotope data. *Gondwana Research*, 39, 401-422.

386 Gardiner, N.J., Searle, M.P., Morley, C.K., Robb, L.J., Whitehouse, M.J., Roberts, N.M.W., Kirkland,
387 C.L. & Spencer, C.J. 2018. The crustal architecture of Myanmar imaged through zircon U-Pb,
388 Lu-Hf and O isotopes: Tectonic and metallogenic implications. *Gondwana Research*, 62, 27-
389 60.

390 Giardini, D. & Woodhouse, J.H. 1986. Horizontal shear flow in the mantle beneath the Tonga arc.
391 *Nature*, 319, 551-555.

392 Gibbons, A.D., Zahirovic, S., Müller, R.D., Whittaker, J.M. & Yatheesh, V. 2015. A tectonic model
393 reconciling evidence for the collisions between India, Eurasia and intra-oceanic arcs of the
394 central-eastern Tethys. *Gondwana Research*, 28, 451-492.

395 Guan, Q., Zhu, D.-C., Zhao, Z.-D., Dong, G.-C., Zhang, L.-L., Li, X.-W., Liu, M., Mo, X.-X., Liu, Y.-S. &
396 Yuan, H.-L. 2012. Crustal thickening prior to 38Ma in southern Tibet: Evidence from lower
397 crust-derived adakitic magmatism in the Gangdese Batholith. *Gondwana Research*, 21, 88-
398 99.

399 Hafkenscheid, E., Wortel, M.J.R. & Spakman, W. 2006. Subduction history of the Tethyan region
400 derived from seismic tomography and tectonic reconstructions. *Journal of Geophysical*
401 *Research: Solid Earth*, 111, n/a-n/a.

402 Hall, R. 2012. Late Jurassic–Cenozoic reconstructions of the Indonesian region and the Indian Ocean.
403 *Tectonophysics*, 570-571, 1-41.

404 Haproff, P.J., Zuza, A.V., Yin, A., Harrison, T.M., Manning, C.E., Dubey, C.S., Ding, L., Wu, C. & Chen, J.
405 2019. Geologic framework of the northern Indo-Burma Ranges and lateral correlation of
406 Himalayan-Tibetan lithologic units across the eastern Himalayan syntaxis. *Geosphere*, 15,
407 856-881.

408 Haproff, P.J., Odlum, M.L., Zuza, A.V., Yin, A. & Stockli, D.F. 2020. Structural and Thermochronologic
409 Constraints on the Cenozoic Tectonic Development of the Northern Indo-Burma Ranges.
410 *Tectonics*, 39, e2020TC006231.

411 Hayes, G.P., Moore, G.L., Portner, D.E., Hearne, M., Flamme, H., Furtney, M. & Smoczyk, G.M. 2018.
412 Slab2, a comprehensive subduction zone geometry model. *Science*, 362, 58-61.

413 Hennig, J., Hall, R. & Armstrong, R.A. 2016. U-Pb zircon geochronology of rocks from west Central
414 Sulawesi, Indonesia: Extension-related metamorphism and magmatism during the early
415 stages of mountain building. *Gondwana Research*, 32, 41-63.

416 Holt, A.F., Royden, L.H., Becker, T.W. & Faccenna, C. 2018. Slab interactions in 3-D subduction
417 settings: The Philippine Sea Plate region. *Earth and Planetary Science Letters*, 489, 72-83.

418 Hosseini, K., Matthews, K.J., Sigloch, K., Shephard, G.E., Domeier, M. & Tsekhmistrenko, M. 2018.
419 SubMachine: Web-Based Tools for Exploring Seismic Tomography and Other Models of
420 Earth's Deep Interior. *Geochemistry, Geophysics, Geosystems*, 19, 1464-1483.

421 Hosseini, K., Sigloch, K., Tsekhmistrenko, M., Zaheri, A., Nissen-Meyer, T. & Igel, H. 2020. Global
422 mantle structure from multi-frequency tomography using P, PP and P-diffracted waves.
423 *Geophysical Journal International*, 220, 96-141.

424 Hu, X., Garzanti, E., Wang, J., Huang, W., An, W. & Webb, A. 2016. The timing of India-Asia collision
425 onset – Facts, theories, controversies. *Earth-Science Reviews*, 160, 264-299.

426 Huang, W., Dupont-Nivet, G., Lippert, P.C., Hinsbergen, D.J.J., Dekkers, M.J., Waldrip, R., Ganerød,
427 M., Li, X., Guo, Z. & Kapp, P. 2015. What was the Paleogene latitude of the Lhasa terrane? A
428 reassessment of the geochronology and paleomagnetism of Linzizong volcanic rocks
429 (Linzhou basin, Tibet). *Tectonics*, 34, 594-622.

430 Ingalls, M., Rowley, D.B., Currie, B. & Colman, A.S. 2016. Large-scale subduction of continental crust
431 implied by India–Asia mass-balance calculation. *Nature Geoscience*, 9, 848.

432 Jacob, J., Dymant, J. & Yatheesh, V. 2014. Revisiting the structure, age, and evolution of the Wharton
433 Basin to better understand subduction under Indonesia. *Journal of Geophysical Research:*
434 *Solid Earth*, 119, 169-190.

435 Jagoutz, O., Royden, L., Holt, A.F. & Becker, T.W. 2015. Anomalously fast convergence of India and
436 Eurasia caused by double subduction. *Nature Geoscience*, 8, 475.

437 Jagoutz, O., Bouilhol, P., Schaltegger, U. & Müntener, O. 2018. The isotopic evolution of the Kohistan
438 Ladakh arc from subduction initiation to continent arc collision. *Geological Society, London,*
439 *Special Publications*, 483.

440 Khin, K., Zaw, K., Aung, L.T., Barber, A.J., Zaw, K. & Crow, M.J. 2017. Geological and tectonic
441 evolution of the Indo-Myanmar Ranges (IMR) in the Myanmar region. *In: Barber, A. J., Zaw,*
442 *K. & Crow, M. J. (eds.) Myanmar: Geology, Resources and Tectonics.* The Geological Society
443 of London. 48, 65-79.

444 Lamont, T.N., Searle, M.P., Hacker, B.R., Htun, K., Htun, K.M., Morley, C.K., Waters, D.J. & White,
445 R.W. 2021. Late Eocene-Oligocene granulite facies garnet-sillimanite migmatites from the
446 Mogok Metamorphic belt, Myanmar, and implications for timing of slip along the Sagaing
447 Fault. *Lithos*, 106027.

448 Le Dain, A.Y., Tapponnier, P. & Molnar, P. 1984. Active faulting and tectonics of Burma and
449 surrounding regions. *Journal of Geophysical Research: Solid Earth*, 89, 453-472.

450 Li, C., van der Hilst, R.D., Engdahl, E.R. & Burdick, S. 2008a. A new global model for P wave speed
451 variations in Earth's mantle. *Geochemistry, Geophysics, Geosystems*, 9.

452 Li, C., van der Hilst, R.D., Meltzer, A.S. & Engdahl, E.R. 2008b. Subduction of the Indian lithosphere
453 beneath the Tibetan Plateau and Burma. *Earth and Planetary Science Letters*, 274, 157-168.

454 Li, Z., Ding, L., Zaw, T., Wang, H., Cai, F., Yao, W., Xiong, Z., Sein, K. & Yue, Y. 2020. Kinematic
455 evolution of the West Burma block during and after India-Asia collision revealed by
456 paleomagnetism. *Journal of Geodynamics*, 134, 101690.

457 Licht, A., Dupont-Nivet, G., Win, Z., Swe, H.H., Kaythi, M., Roperch, P., Ugrai, T., Littell, V., Park, D.,
458 Westerweel, J., Jones, D., Poblete, F., Aung, D.W., Huang, H., Hoorn, C. & Sein, K. 2018.
459 Paleogene evolution of the Burmese forearc basin and implications for the history of India-
460 Asia convergence. *GSA Bulletin*, 131, 730-748.

461 Licht, A., Win, Z., Westerweel, J., Cogné, N., Morley, C.K., Chantpraprasert, S., Poblete, F., Ugrai, T.,
462 Nelson, B., Aung, D.W. & Dupont-Nivet, G. 2020. Magmatic history of central Myanmar and
463 implications for the evolution of the Burma Terrane. *Gondwana Research*, 87, 303-319.

464 Lin, T.-H., Mitchell, A.H.G., Chung, S.-L., Tan, X.-B., Tang, J.-T., Oo, T. & Wu, F.-Y. 2019. Two parallel
465 magmatic belts with contrasting isotopic characteristics from southern Tibet to Myanmar:
466 zircon U–Pb and Hf isotopic constraints. *Journal of the Geological Society*, 176, 574-587.

467 Liu, L., Spasojević, S. & Gurnis, M. 2008. Reconstructing Farallon Plate Subduction Beneath North
468 America Back to the Late Cretaceous. *Science*, 322, 934-938.

469 Ma, L., Wang, B.-D., Jiang, Z.-Q., Wang, Q., Li, Z.-X., Wyman, D.A., Zhao, S.-R., Yang, J.-H., Gou, G.-N.
470 & Guo, H.-F. 2014. Petrogenesis of the Early Eocene adakitic rocks in the Napuri area,
471 southern Lhasa: Partial melting of thickened lower crust during slab break-off and
472 implications for crustal thickening in southern Tibet. *Lithos*, 196-197, 321-338.

473 Macdonald, A.S., Barr, S.M., Miller, B.V., Reynolds, P.H., Rhodes, B.P. & Yokart, B. 2010. P–T–t
474 constraints on the development of the Doi Inthanon metamorphic core complex domain and

475 implications for the evolution of the western gneiss belt, northern Thailand. *Journal of Asian*
476 *Earth Sciences*, 37, 82-104.

477 Martin, C.R., Jagoutz, O., Upadhyay, R., Royden, L.H., Eddy, M.P., Bailey, E., Nichols, C.I.O. & Weiss,
478 B.P. 2020. Paleocene latitude of the Kohistan–Ladakh arc indicates multistage India–Eurasia
479 collision. *Proceedings of the National Academy of Sciences*, 117, 29487-29494.

480 Matthews, K.J., Maloney, K.T., Zahirovic, S., Williams, S.E., Seton, M. & Müller, R.D. 2016. Global
481 plate boundary evolution and kinematics since the late Paleozoic. *Global and Planetary*
482 *Change*, 146, 226-250.

483 Min, M. 2007. *Thermochronology applied to strike–slip zones Central America and Myanmar*. PhD
484 thesis.

485 Min, S., Watkinson, I.M., Tun, S.T., Naing, W. & Swe, T.L. 2017. The Kyaukkyan Fault, Myanmar. *In:*
486 Barber, A. J., Zaw, K. & Crow, M. J. (eds.) *Myanmar: Geology, Resources and Tectonics*. The
487 Geological Society of London. 48, 453-471.

488 Molnar, P. & Stock, J.M. 2009. Slowing of India's convergence with Eurasia since 20 Ma and its
489 implications for Tibetan mantle dynamics. *Tectonics*, 28.

490 Morley, C.K. 2012. Late Cretaceous–Early Palaeogene tectonic development of SE Asia. *Earth-Science*
491 *Reviews*, 115, 37-75.

492 Morley, C.K. & Arboit, F. 2019. Dating the onset of motion on the Sagaing fault: Evidence from
493 detrital zircon and titanite U-Pb geochronology from the North Minwun Basin, Myanmar.
494 *Geology*, 47, 581-585.

495 Morley, C.K., Chantraprasert, S., Kongchum, J. & Chenoll, K. 2021. The West Burma Terrane, a review
496 of recent paleo-latitude data, its geological implications and constraints. *Earth-Science*
497 *Reviews*, 220, 103722.

498 Müller, R.D., Cannon, J., Qin, X., Watson, R.J., Gurnis, M., Williams, S., Pfaffelmoser, T., Seton, M.,
499 Russell, S.H.J. & Zahirovic, S. 2018. GPlates: Building a Virtual Earth Through Deep Time.
500 *Geochemistry, Geophysics, Geosystems*, 19, 2243-2261.

501 Müller, R.D., Zahirovic, S., Williams, S.E., Cannon, J., Seton, M., Bower, D.J., Tetley, M., Heine, C., Le
502 Breton, E., Liu, S., Russell, S.H.J., Yang, T., Leonard, J. & Gurnis, M. 2019. A global plate model
503 including lithospheric deformation along major rifts and orogens since the Triassic.
504 *Tectonics*, 38, 1884–1907.

505 Najman, Y., Sobel, E.R., Millar, I., Stockli, D.F., Govin, G., Lisker, F., Garzanti, E., Limonta, M., Vezzoli,
506 G., Copley, A., Zhang, P., Szymanski, E. & Kahn, A. 2020. The exhumation of the Indo-Burman
507 Ranges, Myanmar. *Earth and Planetary Science Letters*, 530, 115948.

508 Ng, S.W.-P., Whitehouse, M.J., Searle, M.P., Robb, L.J., Ghani, A.A., Chung, S.-L., Oliver, G.J.H., Sone,
509 M., Gardiner, N.J. & Roselee, M.H. 2015. Petrogenesis of Malaysian granitoids in the
510 Southeast Asian tin belt: Part 2. U-Pb zircon geochronology and tectonic model. *GSA Bulletin*,
511 127, 1238-1258.

512 Obayashi, M., Yoshimitsu, J., Nolet, G., Fukao, Y., Shiobara, H., Sugioka, H., Miyamachi, H. & Gao, Y.
513 2013. Finite frequency whole mantle P wave tomography: Improvement of subducted slab
514 images. *Geophysical Research Letters*, 40, 5652-5657.

515 Österle, J.E., Klötzli, U., Stockli, D.F., Palzer-Khomenko, M. & Kanjanapayont, P. 2019. New age
516 constraints on the Lan Sang gneiss complex, Thailand, and the timing of activity of the Mae
517 Ping shear zone from in-situ and depth-profile zircon and monazite U-Th-Pb geochronology.
518 *Journal of Asian Earth Sciences*, 181, 103886.

519 Palin, R.M., Searle, M.P., Morley, C.K., Charusiri, P., Horstwood, M.S.A. & Roberts, N.M.W. 2013.
520 Timing of metamorphism of the Lansang gneiss and implications for left-lateral motion along
521 the Mae Ping (Wang Chao) strike-slip fault, Thailand. *Journal of Asian Earth Sciences*, 76,
522 120-136.

523 Palin, R.M., Searle, M.P., St-Onge, M.R., Waters, D.J., Roberts, N.M.W., Horstwood, M.S.A., Parrish,
524 R.R., Weller, O.M., Chen, S. & Yang, J. 2014. Monazite geochronology and petrology of

kyanite- and sillimanite-grade migmatites from the northwestern flank of the eastern Himalayan syntaxis. *Gondwana Research*, 26, 323-347.

Parsons, A.J., Hosseini, K., Palin, R. & Sigloch, K. 2020. Geological, geophysical and plate kinematic constraints for models of the India-Asia collision and the post-Triassic central Tethys oceans. *Earth-Science Reviews*, 103084.

Patriat, P. & Achache, J. 1984. India–Eurasia collision chronology has implications for crustal shortening and driving mechanism of plates. *Nature*, 311, 615-621.

Replumaz, A., Capitanio, F.A., Guillot, S., Negredo, A.M. & Villaseñor, A. 2014. The coupling of Indian subduction and Asian continental tectonics. *Gondwana Research*, 26, 608-626.

Schaeffer, A.J. & Lebedev, S. 2013. Global shear speed structure of the upper mantle and transition zone. *Geophysical Journal International*, 194, 417-449.

Schellart, W.P. 2005. Influence of the subducting plate velocity on the geometry of the slab and migration of the subduction hinge. *Earth and Planetary Science Letters*, 231, 197-219.

Schellart, W.P., Stegman, D.R. & Freeman, J. 2008. Global trench migration velocities and slab migration induced upper mantle volume fluxes: Constraints to find an Earth reference frame based on minimizing viscous dissipation. *Earth-Science Reviews*, 88, 118-144.

Searle, M.P., Noble, S.R., Cottle, J.M., Waters, D.J., Mitchell, A.H.G., Hlaing, T. & Horstwood, M.S.A. 2007. Tectonic evolution of the Mogok metamorphic belt, Burma (Myanmar) constrained by U-Th-Pb dating of metamorphic and magmatic rocks. *Tectonics*, 26.

Searle, M.P., Elliott, J.R., Phillips, R.J. & Chung, S.L. 2011. Crustal–lithospheric structure and continental extrusion of Tibet. *Journal of the Geological Society*, 168, 633-672.

Searle, M.P., Whitehouse, M.J., Robb, L.J., Ghani, A.A., Hutchison, C.S., Sone, M., Ng, S.W.-P., Roselee, M.H., Chung, S.-L. & Oliver, G.J.H. 2012. Tectonic evolution of the Sibumasu–Indochina terrane collision zone in Thailand and Malaysia: constraints from new U–Pb zircon chronology of SE Asian tin granitoids. *Journal of the Geological Society*, 169, 489-500.

Searle, M.P., Morley, C.K., Waters, D.J., Gardiner, N.J., Kyi Htun, U., Nu, T.T. & Robb, L.J. 2017. Tectonic and metamorphic evolution of the Mogok Metamorphic and Jade Mines belts and ophiolitic terranes of Burma (Myanmar). In: Barber, A. J., Zaw, K. & Crow, M. J. (eds.) *Myanmar: Geology, Resources and Tectonics*. The Geological Society of London. 48, 261-293.

Searle, M.P., Garber, J.M., Hacker, B.R., Htun, K., Gardiner, N.J., Waters, D.J. & Robb, L.J. 2020. Timing of Syenite-Charnockite Magmatism and Ruby and Sapphire Metamorphism in the Mogok Valley Region, Myanmar. *Tectonics*, 39, e2019TC005998.

Seton, M., Müller, R.D., Zahirovic, S., Williams, S., Wright, N.M., Cannon, J., Whittaker, J.M., Matthews, K.J. & McGirr, R. 2020. A Global Data Set of Present-Day Oceanic Crustal Age and Seafloor Spreading Parameters. *Geochemistry, Geophysics, Geosystems*, 21, e2020GC009214.

Sigloch, K. & Mihalyuk, M.G. 2017. Mantle and geological evidence for a Late Jurassic–Cretaceous suture spanning North America. *GSA Bulletin*, 129, 1489-1520.

Simmons, N.A., Myers, S.C., Johannesson, G. & Matzel, E. 2012. LLNL-G3Dv3: Global P wave tomography model for improved regional and teleseismic travel time prediction. *Journal of Geophysical Research: Solid Earth*, 117.

Simpson, A., Glorie, S., Morley, C.K., Roberts, N.M.W., Gillespie, J. & Lee, J.K. 2021. In-situ calcite U-Pb geochronology of hydrothermal veins in Thailand: New constraints on Indosinian and Cenozoic deformation. *Journal of Asian Earth Sciences*, 206, 104649.

Sloan, R.A., Elliott, J.R., Searle, M.P., Morley, C.K., Barber, A.J., Zaw, K. & Crow, M.J. 2017. Active tectonics of Myanmar and the Andaman Sea. In: Barber, A. J., Zaw, K. & Crow, M. J. (eds.) *Myanmar: Geology, Resources and Tectonics*. The Geological Society of London. 48, 19-52.

Smyth, H.R., Hall, R., Nichols, G.J., Draut, A.E., Clift, P.D. & Scholl, D.W. 2008. Cenozoic volcanic arc history of East Java, Indonesia: The stratigraphic record of eruptions on an active continental margin. In: Draut, A. E., Clift, P. D. & Scholl, D. W. (eds.) *Formation and Applications of the Sedimentary Record in Arc Collision Zones*. Geological Society of America. 436, 199-222.

576 Spakman, W., Chertova, M.V., van den Berg, A. & van Hinsbergen, D.J.J. 2018. Puzzling features of
577 western Mediterranean tectonics explained by slab dragging. *Nature Geoscience*, 11, 211-
578 216.

579 Steinberger, B., Torsvik, T.H. & Becker, T.W. 2012. Subduction to the lower mantle - a comparison
580 between geodynamic and tomographic models. *Solid Earth*, 3, 415-432.

581 Torsvik, T.H., Müller, R.D., Van der Voo, R., Steinberger, B. & Gaina, C. 2008. Global plate motion
582 frames: Toward a unified model. *Reviews of Geophysics*, 46.

583 Torsvik, T.H., Amundsen, H., Hartz, E.H., Corfu, F., Kuznir, N., Gaina, C., Doubrovine, P.V.,
584 Steinberger, B., Ashwal, L.D. & Jamtveit, B. 2013. A Precambrian microcontinent in the
585 Indian Ocean. *Nature Geoscience*, 6, 223-227.

586 van de Lagemaat, S.H.A., van Hinsbergen, D.J.J., Boschman, L.M., Kamp, P.J.J. & Spakman, W. 2018.
587 Southwest Pacific Absolute Plate Kinematic Reconstruction Reveals Major Cenozoic Tonga-
588 Kermadec Slab Dragging. *Tectonics*, 37, 2647-2674.

589 van der Meer, D.G., Spakman, W., van Hinsbergen, D.J.J., Amaru, M.L. & Torsvik, T.H. 2010. Towards
590 absolute plate motions constrained by lower-mantle slab remnants. *Nature Geoscience*, 3,
591 36.

592 van der Meer, D.G., van Hinsbergen, D.J.J. & Spakman, W. 2018. Atlas of the underworld: Slab
593 remnants in the mantle, their sinking history, and a new outlook on lower mantle viscosity.
594 *Tectonophysics*, 723, 309-448.

595 van Hinsbergen, D.J.J., Lippert, P.C., Li, S., Huang, W., Advokaat, E.L. & Spakman, W. 2019.
596 Reconstructing Greater India: Paleogeographic, kinematic, and geodynamic perspectives.
597 *Tectonophysics*, 760, 69-94.

598 Watkinson, I., Elders, C., Batt, G., Jourdan, F., Hall, R. & McNaughton, N.J. 2011. The timing of strike-
599 slip shear along the Ranong and Khlong Marui faults, Thailand. *Journal of Geophysical*
600 *Research: Solid Earth*, 116.

601 Westerweel, J., Roperch, P., Licht, A., Dupont-Nivet, G., Win, Z., Poblete, F., Ruffet, G., Swe, H.H., Thi,
602 M.K. & Aung, D.W. 2019. Burma Terrane part of the Trans-Tethyan arc during collision with
603 India according to palaeomagnetic data. *Nature Geoscience*, 12, 863-868.

604 Westerweel, J., Licht, A., Cogné, N., Roperch, P., Dupont-Nivet, G., Kay Thi, M., Swe, H.H., Huang, H.,
605 Win, Z. & Wa Aung, D. 2020. Burma Terrane Collision and Northward Indentation in the
606 Eastern Himalayas Recorded in the Eocene-Miocene Chindwin Basin (Myanmar). *Tectonics*,
607 39, e2020TC006413.

608 White, L.T., Hall, R., Armstrong, R.A., Barber, A.J., BouDagher Fadel, M., Baxter, A., Wakita, K.,
609 Manning, C. & Soesilo, J. 2017. The geological history of the Latimojong region of western
610 Sulawesi, Indonesia. *Journal of Asian Earth Sciences*, 138, 72-91.

611 Wu, J., Suppe, J., Lu, R. & Kanda, R. 2016. Philippine Sea and East Asian plate tectonics since 52 Ma
612 constrained by new subducted slab reconstruction methods. *Journal of Geophysical*
613 *Research: Solid Earth*, 121, 4670-4741.

614 Zhang, X., Tien, C.-Y., Chung, S.-L., Maulana, A., Mawaleda, M., Chu, M.-F. & Lee, H.-Y. 2020. A Late
615 Miocene magmatic flare-up in West Sulawesi triggered by Banda slab rollback. *GSA Bulletin*,
616 132, 2517-2528.

617 Zhang, Z., Dong, X., Xiang, H., Ding, H., He, Z. & Liou, J.G. 2015. Reworking of the Gangdese magmatic
618 arc, southeastern Tibet: post-collisional metamorphism and anatexis. *Journal of*
619 *Metamorphic Geology*, 33, 1-21.

620 Zhang, Z.M., Zhao, G.C., Santosh, M., Wang, J.L., Dong, X. & Liou, J.G. 2010. Two stages of granulite
621 facies metamorphism in the eastern Himalayan syntaxis, south Tibet: petrology, zircon
622 geochronology and implications for the subduction of Neo-Tethys and the Indian continent
623 beneath Asia. *Journal of Metamorphic Geology*, 28, 719-733.

624 Zhu, D.-C., Wang, Q., Chung, S.-L., Cawood, P.A. & Zhao, Z.-D. 2018. Gangdese magmatism in
625 southern Tibet and India-Asia convergence since 120 Ma. *Geological Society, London,*
626 *Special Publications*, 483, SP483.14.

627

628 **Figure 1.** Tectonic map of the Indian Ocean, showing outlines of Anomalies II, III and VII, and Late
629 Cretaceous-Cenozoic subduction magmatism. Plate boundaries, slab-depth profile, and seafloor
630 isochrons drawn from Bird (2003), Hayes et al. (2018) and Müller et al. (2019).

631 **Figure 2.** Select seismic tomography depth slices (a-c) and cross sections (d-f) with outlines of
632 seismic anomalies from P-wave tomography model UU-P07 (Amaru, 2007). (g-i) Outlines of
633 anomalies used for slab restorations (Figs. 3-4), are based on interpretation of six tomography
634 models and Slab2.0 model (see Supporting Information and Supporting Dataset).

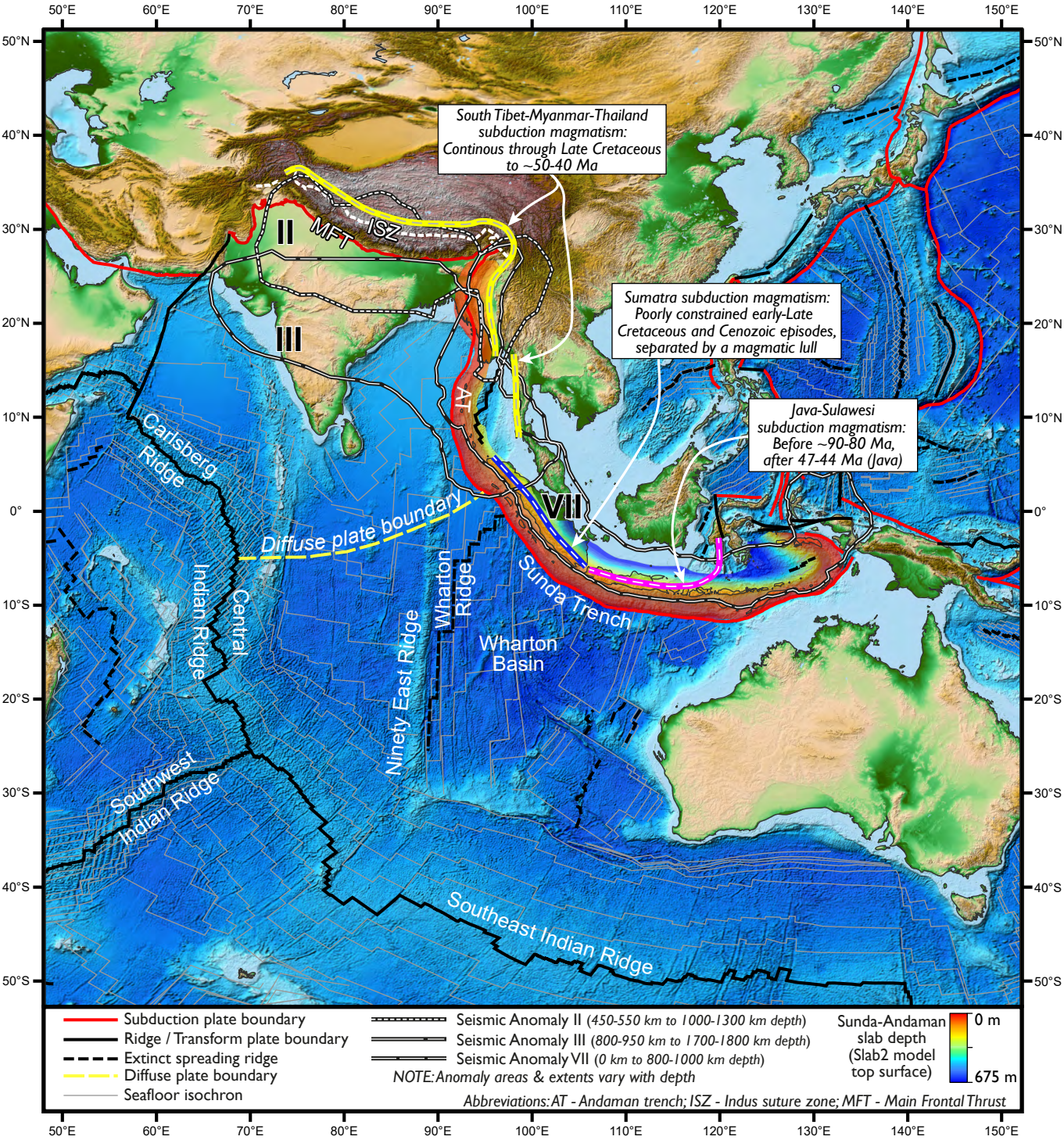
635 **Figure 3.** (a-b) Reconstruction of two-stage India-Asia collision modified from Müller et al. (2019),
636 including Anomaly VII slab restoration. (c) Plate kinematics (Torsvik et al., 2008, Doubrovine et al.,
637 2012, Müller et al., 2019) highlighting plate network reorganisation events following Second
638 Collision at 45-40 Ma.

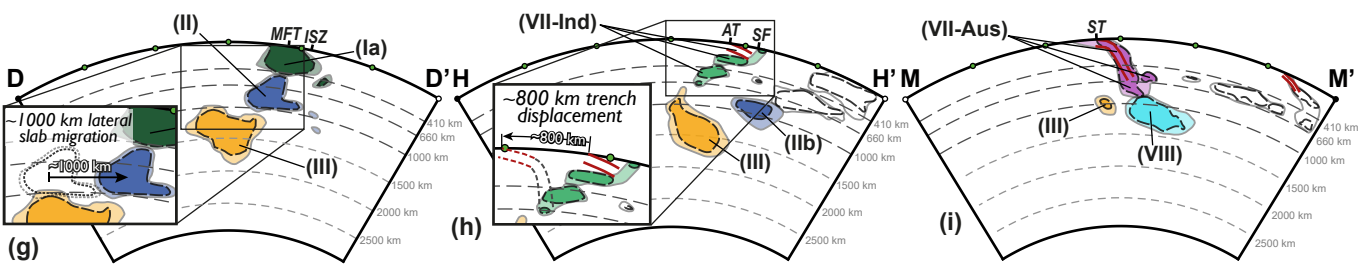
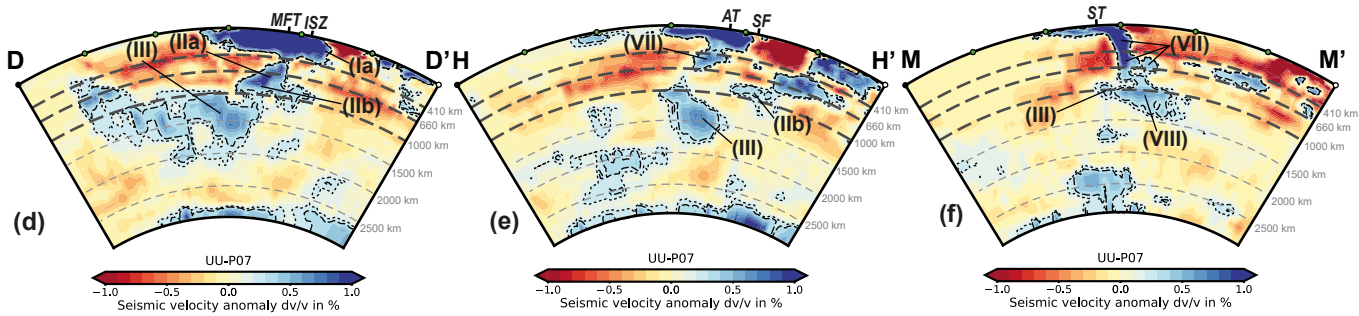
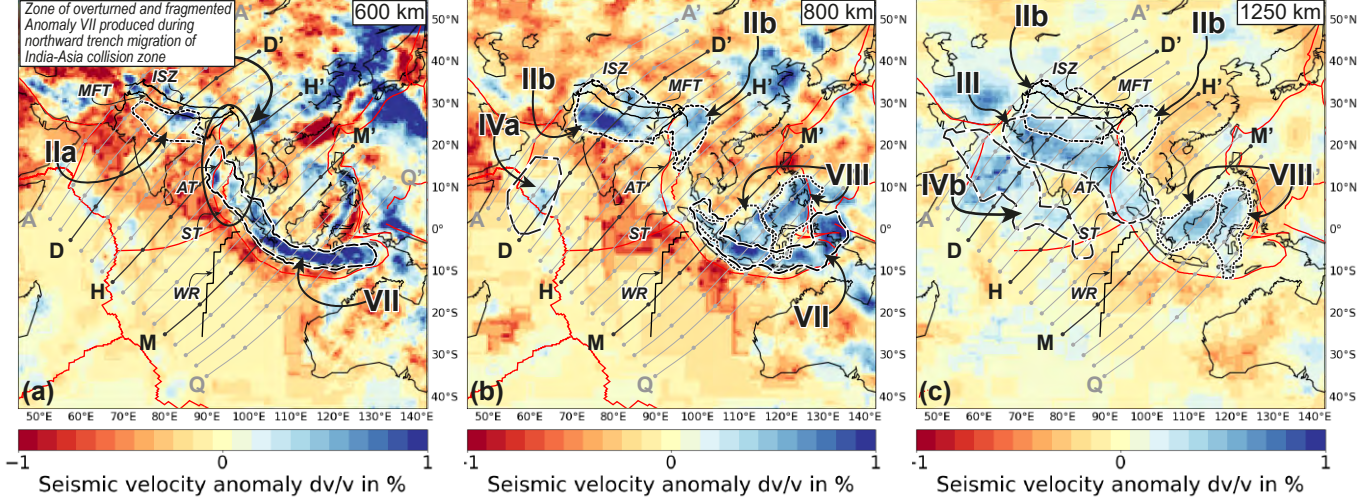
639 **Figure 4.** Cartoon representations of slab kinematics since Second Collision (45-40 Ma), looking
640 southwest. Anomaly VII divides into Indian (green) and Australian (purple) slabs, either side of the
641 extinct Wharton ridge. Coloured arrows show approximate slab motions. LSM of Anomaly II (blue)
642 occurs between (a) Second Collision and (b) slab break-off. Indian plate Anomaly VII slab (green) is
643 overturned and fragmented during northeast migration of India-Eurasia collision zone.

644

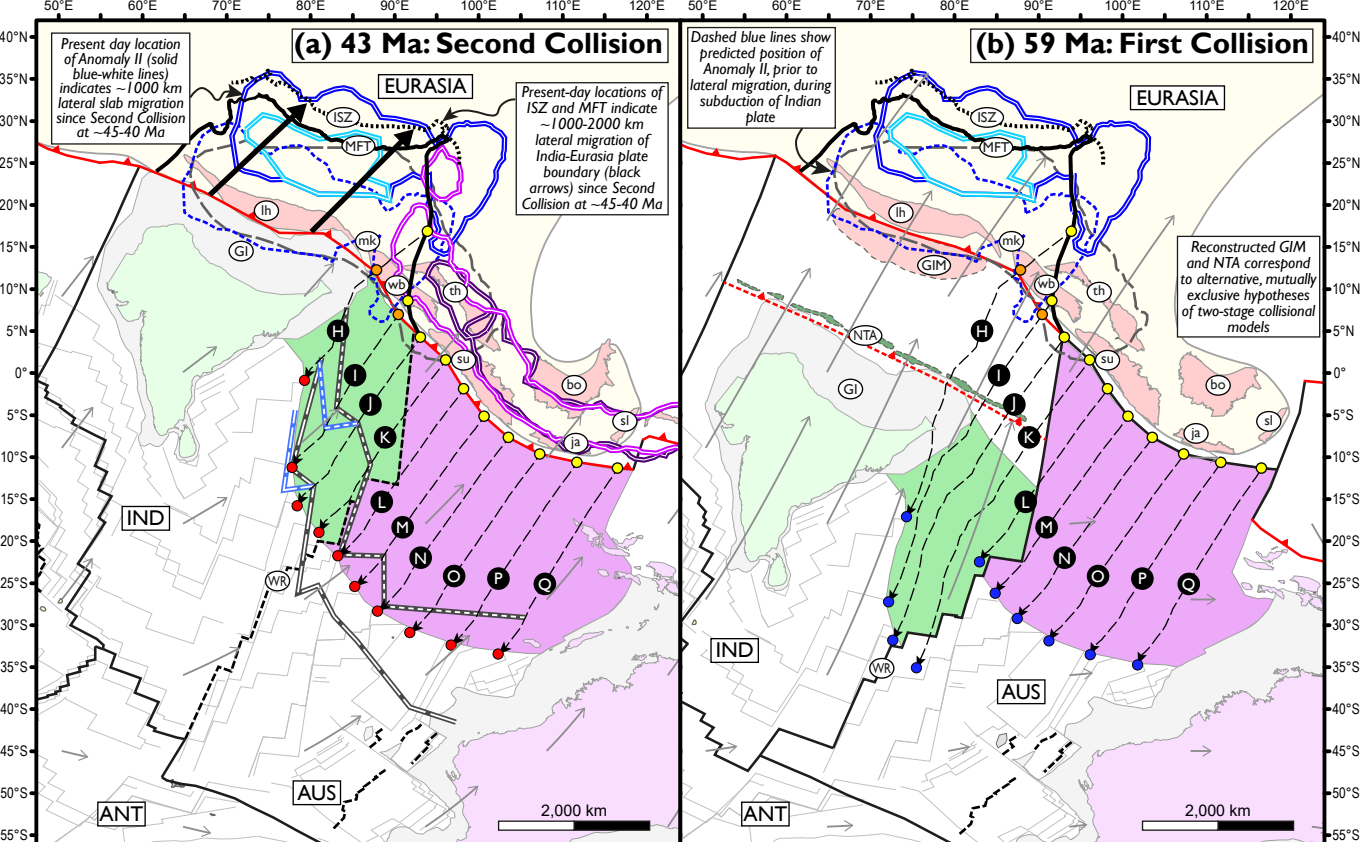
645

646





NOTE: Anomaly VII is divided into Indian plate (VII-Ind) and Australian plate (VII-Aus)



(a) 43 Ma: Second Collision

(b) 59 Ma: First Collision

Present day location of Anomaly II (solid blue-white lines) indicates ~1000 km lateral slab migration since Second Collision at ~45-40 Ma

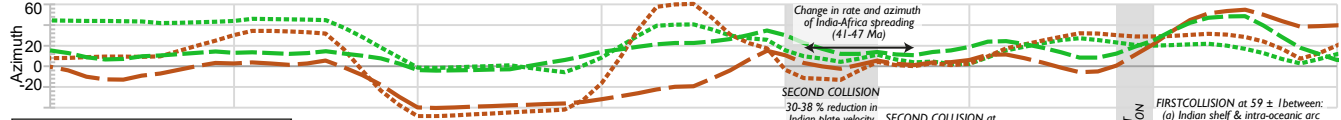
Present-day locations of ISZ and MFT indicate ~1000-2000 km lateral migration of India-Eurasia plate boundary (black arrows) since Second Collision at ~45-40 Ma

Dashed blue lines show predicted position of Anomaly II, prior to lateral migration, during subduction of Indian plate

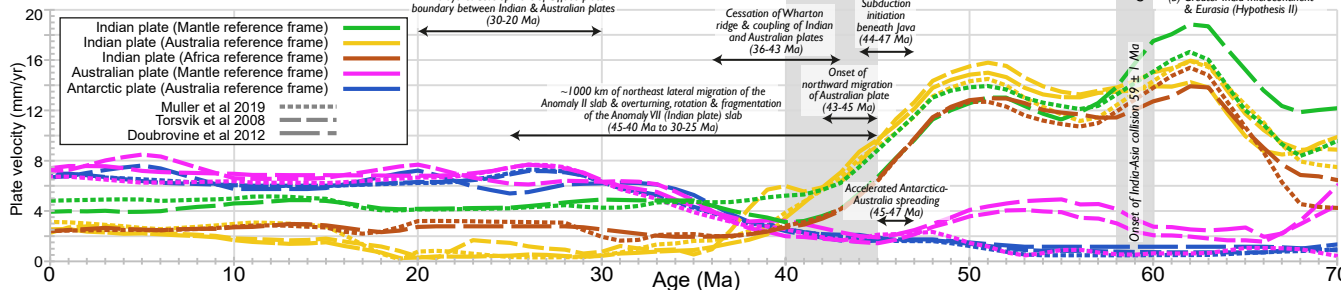
Reconstructed GIM and NTA correspond to alternative, mutually exclusive hypotheses of two-stage collisional models

- ▲— Subduction plate boundary
- Spreading ridge / Transform plate boundary
- - - Extinct spreading ridge
- - - Fracture zone
- Seafloor isochron
- Plate velocity (relative to fixed mantle)
- Trench location at 0 Ma
- Restored trench location at 59-43 Ma
- - -▲- - - Subduction boundary - two-stage collision Hypothesis I only
- Anomaly VII (~300 km to 600-700 km depth)
- Anomaly VII (600-700 km to ~1000 km depth)
- Anomaly II (450-550 km to 700-800 km depth)
- Anomaly II (700-800 km to 1000-1300 km depth)
- - - Anomaly II location prior to lateral migration (predicted)
- - - Anomaly III (800-900 km to 1600-1700 km depth)
- NOTE: Anomaly VII at 0-300 km depth is omitted for clarity
- Restored Anomaly VII-Aus slab (Australian plate, subducted since ~43 Ma)
- Restored Anomaly VII-Ind slab (Indian plate, subducted since ~43 Ma)
- Maximum restored length of Anomaly VII slab, based on cross-section restoration
- Minimum restored length of Anomaly VII slab, based on cross-section restoration
- - - Maximum restored length of Anomaly VII slab + trench migration
- - - Minimum restored length of Anomaly VII slab + trench migration
- Top of restored Anomaly VII slab at 43 Ma, based on plate motions
- Top of restored Anomaly VII slab at 59 Ma, based on plate motions
- - - Plate motion path (letters correspond to cross sections)
- NOTE: Cross-section based Anomaly VII restorations follow plate motion paths
- Continental shelf (India and Australia)
- Eurasian continent (Paleo-Pacific margin is approximated)
- Restored locations of present-day coastlines and continental blocks (approximated)
- Present day location of India-Eurasia plate boundary
- - - Present day location of ISZ
- Approximated migration of India-Eurasia plate boundary since 43 Ma
- Neotethys intra-oceanic arc (NTA) - two-stage collision Hypothesis I only
- Greater India microcontinent (GIM) - two-stage collision Hypothesis II only

Abbreviations: ANT - Antarctic plate; AUS - Australian plate; bo - Borneo; GI - Greater India; GIM - Greater India microcontinent; IND - Indian plate; ISZ - Indus suture zone; ja - Java; lh - Lhasa block; MFT - Main frontal thrust; mk - Mogok metamorphic belt (northeast Myanmar); NTA - Neotethys intra-oceanic arc; sl - Sulawesi; su - Sumatra; th - Thailand-Malaysia; wb - West Burma block; WR - Wharton ridge



(c) Plate kinematics

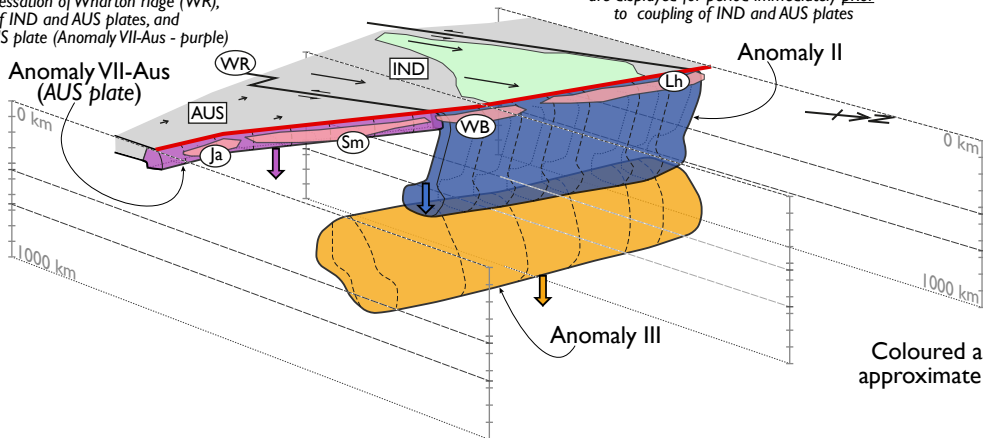


- Indian plate (Mantle reference frame)
- Indian plate (Australia reference frame)
- Indian plate (Africa reference frame)
- Australian plate (Mantle reference frame)
- Antarctic plate (Australia reference frame)
- Muller et al 2019
- Torsvik et al 2008
- Dobrovine et al 2012

(a) 45-40 Ma

"Second Collision" of India with Eurasia at ~45-40 Ma is followed by cessation of Wharton ridge (WR), coupling of IND and AUS plates, and subduction of AUS plate (Anomaly VII-Aus - purple)

NOTE: plate motions (dark grey arrows) are displayed for period immediately *prior* to coupling of IND and AUS plates



(b) 30-25 Ma

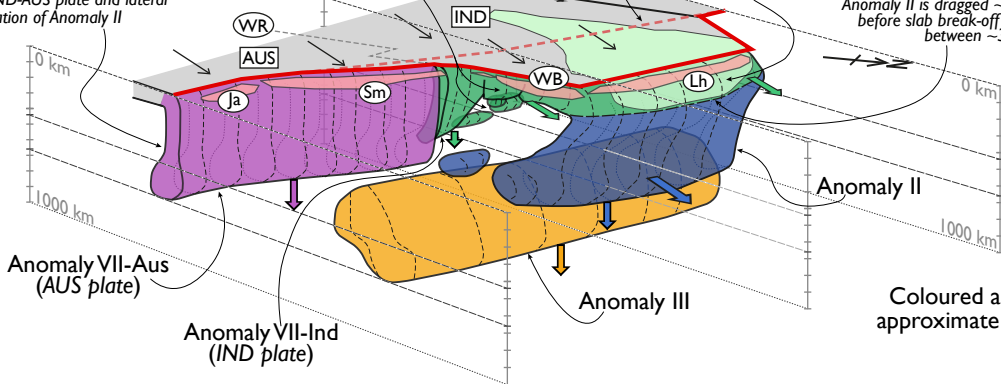
Lateral migration of India-Eurasia subduction zone results in overturning, fragmentation & clockwise rotation of subducting IND oceanic lithosphere (Anomaly VII-Ind - green) via 'unzipping' of Wharton ridge (WR) during subduction

Subduction of AUS oceanic lithosphere (Anomaly VII-Aus - purple) drives northeast motion of IND-AUS plate and lateral migration of Anomaly II

Location of Eurasian plate boundary at 43 Ma

Bouoyancy of IND continental lithosphere (light green) keeps Indian plate afloat during northeast plate motion

Anomaly II is dragged ~1,000 km northwards before slab break-off (thick dashed line) between ~30-25 Ma



(c) 0 Ma

Eurasian plate boundary west of Wharton ridge remained stationary during subduction, resulting in a vertical slab

Location of Eurasian plate boundary at 43 Ma

Lateral migration of India-Eurasia plate boundary and Anomaly VII-Ind (IND plate) slab continues after break-off of Anomaly II slab

